Prediction of Methane Destructive Efficiency of a Gas Flare using CFD with Adaptive Mesh Refinement and Detailed Chemistry

Lu Li,[1] Sameera Wijeyakulasuriya,[1] and Jianhui Hong[2]

[1]*Convergent Science Inc, Madison, WI, USA*
[2]*Cimarron Energy Inc, Houston, TX, USA*

(Dated: September 22, 2025)

Methane, a potent greenhouse gas, is often flared in oil and gas operations to prevent its direct release into the atmosphere. Achieving a high destruction and removal efficiency (DRE) during flaring is crucial for minimizing environmental impact. This study demonstrates the application of computational fluid dynamics (CFD) to assess the destruction of methane in flare systems under realistic operating conditions. Reactive flow simulations are performed using CONVERGE CFD software, which incorporates RANS turbulence modeling and the SAGE detailed chemistry solver to accurately simulate the combustion process of the gas flare. The simulation considers realistic natural gas composition, measured fuel and air flow rates, crosswind conditions, and air entrainment, offering insights into how these variables influence the efficiency of methane destruction. The results show that with optimal air assistance, the flare system can achieve a methane destruction efficiency on par with the measurements, underscoring the potential of CFD in evaluating and improving flare system performance.

I. INTRODUCTION

Gas flaring is a routine safety practice in the oil and gas industry used to safely burn off excess hydrocarbons during normal operations, maintenance, and emergencies. Although flaring is intended to convert methane and other hydrocarbons completely to carbon dioxide and water, incomplete combustion often occurs under real-world conditions. Factors such as insufficient oxygen supply, flame instability, and poor mixing can cause unburned methane to be released along with other pollutants. Since methane has a much higher global warming potential than carbon dioxide, even small emissions from flaring can have significant environmental impacts. Additionally, flaring contributes to local air pollution through soot and other harmful byproducts formed during combustion [1]. Therefore, improving flare performance—particularly combustion efficiency (CE) and destruction and removal efficiency (DRE)—is essential to minimize emissions and comply with increasingly stringent environmental regulations.

CE quantifies how completely hydrocarbons are oxidized during combustion, while DRE measures the effectiveness of destroying hazardous compounds such as methane and volatile organic compounds (VOCs). These efficiencies depend on several factors including fuel composition, flare tip design, operating conditions, and meteorological influences. To improve combustion and achieve smokeless operation, assist systems such as steam- and air-assisted flares are widely used. Steam injection adds momentum and suppresses soot by diluting fuel and modifying combustion chemistry [2]; however, it requires a steady steam supply and may pose operational challenges in cold climates due to condensation and freezing. Air-assisted flares [3] offer simpler implementation and flexibility but must be carefully controlled to avoid over-aeration, which can lower flame temperatures and reduce residence times, adversely affecting DRE [4]. Optimizing assist air supply is therefore essential for effective flare operation.

Computational fluid dynamics (CFD) offers a powerful and cost-effective approach to analyze the complex fluid flow, combustion chemistry, heat transfer, and mixing processes within flares. This study employs CFD to investigate the combustion behavior of the Hybrid flare—patent pending by Hong and marketed by Cimarron [5]—under various stoichiometric air flow rates (30%, 50%, 100%, and 150%). The detailed chemistry solver SAGE, which incorporates finite-rate chemical kinetics to enhance predictions of pollutant formation and combustion dynamics, is used for the simulations. This approach enables accurate predictions of flame structure, methane destruction efficiency, and pollutant emissions. The results provide valuable insight into how air delivery assist affects flame stability and combustion performance, informing strategies to optimize flare operation and reduce emissions.

II. EXPERIMENTAL SETUP

The hybrid tandem flare is equipped with two types of gas risers: one for high-pressure (HP) gas and one for low-pressure (LP) gas. The HP gas is typically associated gas, which refers to natural gas that is co-produced during crude oil extraction, while the LP gas consists of vapor released from temporary storage tanks before the crude oil is transported off-site. As illustrated in Fig. 1, the hybrid flare features two HP fuel inlets: a 4-inch line and an 8-inch line. The 4-inch HP inlet feeds the lower section of the central tube and delivers gas through small red tubes

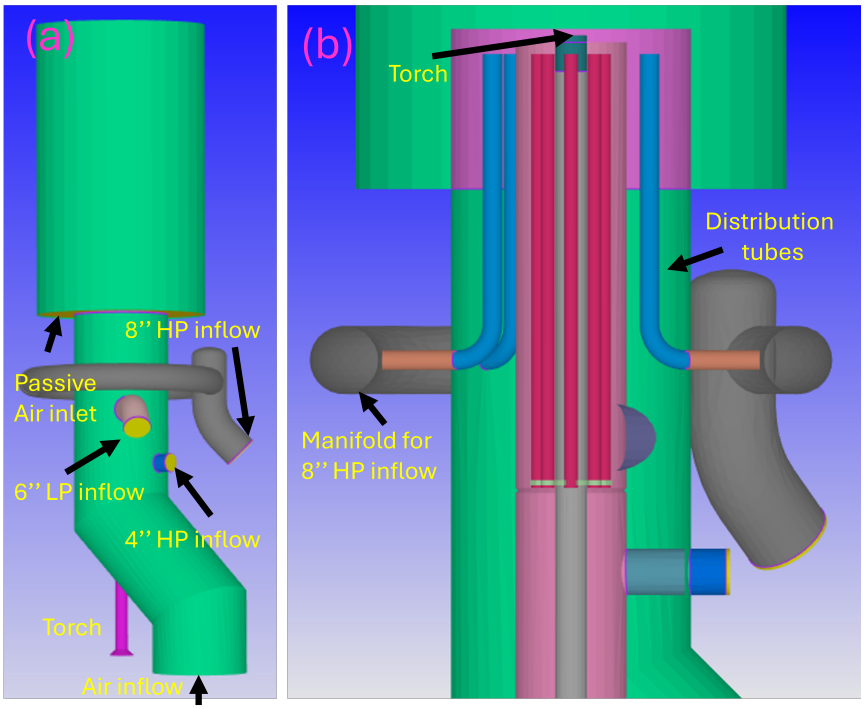

FIG. 1: External (a) and sectional (b) views of Cimarron hybrid tandem flare, with two high-pressure fuel inlets, one low-pressure inlet, air inlet from the bottom, and torch at the center

to the torch, forming high-velocity jets that enhance turbulence and promote fuel-air mixing. The 8-inch HP inlet is connected to a ring-shaped manifold and distributes gas evenly to the torch through larger blue tubes. The 6-inch LP fuel inlet connects to the upper section of the central tube and forms a co-flow with the HP jet from the 4-inch line. Ambient air enters through a dedicated pipe at the bottom and also forms a co-flow with the HP and LP fuel streams, contributing to the overall mixing and combustion process. A cylindrical shroud encloses the upper section of the flare, serving both as a windshield and as an air induction chamber. The momentum of the HP/LP fuel and assist air mixture draws additional air into the shroud through its bottom opening, promoting further mixing and stabilizing the flame. The representative fuel compositions for the HP and LP gas are shown in Table I [6].

TABLE I: Typical composition for HP and LP gas by volume fraction

Name	HP	LP
Methane(CH4)	0.670	0.170
Ethane(C2H6)	0.149	0.230
Propane(C3H8)	0.100	0.310
Butane(C4H10)	0.042	0.180
Pentane(C5H12)	0.013	0.065
Hexane(C6H14)	0.004	0.017
Heptane(C7H16)	0.003	0.015
Carbon Dioxide(CO2)	0.007	0.006
Nitrogen(N2)	0.012	0.007

III. NUMERICAL SETUP

In this study, the commercial code CONVERGE (version 4.0.2) [7] was used for computational fluid dynamics (CFD) simulations. In this section, an overview of geometry setup, grid strategy, physical models used, chemical kinetics mechanism selection, and numerical scheme considerations are discussed.

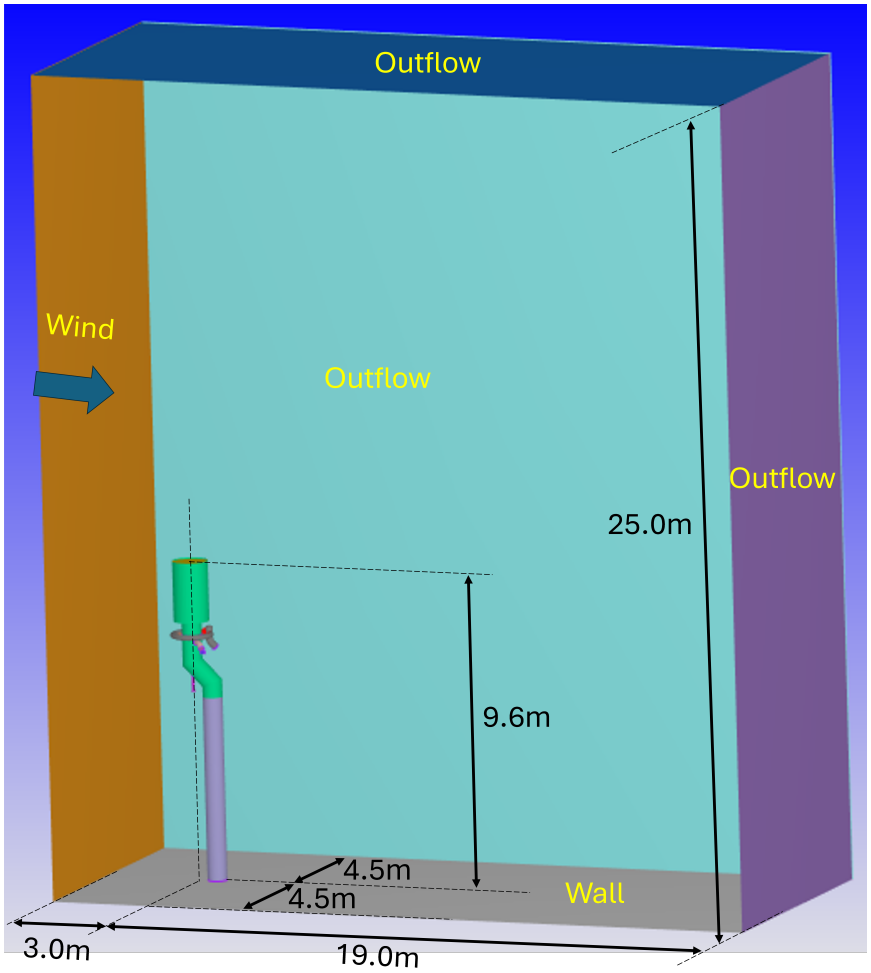

FIG. 2: Computational domain and boundary conditions used

A. Geometry and boundary conditions

The simulation domain is depicted in Fig. 2. A uniform wind with a velocity of 10 miles per hour (mph) enters from the left, where the boundary is defined as a velocity inlet that supplies ambient air. The right-side boundary is set as a pressure outlet. The flare is positioned 3.0 meters from the inlet and 19.0 meters from the outlet, ensuring sufficient space for capturing the complete flame structure, including stabilization, lift-off height, and methane oxidation behavior. Laterally, the flare is placed 4.5 meters from both the front and rear boundaries, which are also defined as pressure outlets to accommodate crossflow entrainment and to minimize boundary effects on the gas flare. The bottom surface of the domain is modeled as a no-slip wall representing the ground. The top boundary is defined as another pressure outlet to allow the upward escape of combustion gases. Gravity is enabled in the simulation, and all pressure outlet boundaries are configured with hydrostatic pressure conditions to properly account for buoyancy effects and the upward movement of hot combustion gases due to density differences.

In this study, the simulation focuses on flow conditions involving only the HP fuel through the 4-inch HP inlet. The fuel flow rate is set at 500 Million Standard Cubic Feet per Day (MSCFD), corresponding to approximately 0.164 m^3/s under standard conditions. The air is introduced through the bottom air-inlet pipe, with the flow rate varied based on specific ratios relative to the stoichiometric air requirement for complete combustion of the HP fuel. The other two fuel inlets—the 8-inch HP line and the 6-inch LP inlet—are treated as wall boundaries and remain inactive during the simulation to mimic the operating conditions modeled here. The torch is simulated as a continuous high-temperature inflow (2000K) with combustion products for the HP fuel gas with an equivalence ratio of 1.

B. Grid setup

The code employs a cut-cell Cartesian meshing approach to dynamically generate the volume mesh at runtime [7]. In these simulations, the base mesh size (largest cell size in the domain) was 400 mm. To accurately resolve the flame front and turbulent flow structures, Adaptive Mesh Refinement (AMR) is activated. Temperature-based AMR is used to capture flame propagation, while velocity-based AMR resolves complex turbulent features, and CH4 mass fraction-based AMR enhances resolution in regions critical to methane destruction. All AMR methods refine the mesh down to a minimum cell size of 12.5 mm. In addition, fixed embeddings are applied to enforce local refinement in geometrically important areas such as the fuel injection tubes. Around the torch region, where combustion is initiated, additional fixed embedding ensures sufficient spatial resolution to capture flame anchoring, ignition dynamics, and early stage jet–air mixing. With the above settings, the simulation reached a maximum cell count of approximately 2.5 million. A maximum Courant–Friedrichs–Lewy (CFL) number of 10 was used, resulting in a time step of $\sim 2 \times 10^{-3}$ seconds.

C. Physical models

The renormalization group k-eps turbulence model [8] was selected to model the turbulence, the O'Rourke and Amsden wall heat transfer model [9]] is used to model heat transfer to the walls, the standard wall function [10] is used to calculate the velocity near the walls. The SAGE detailed chemistry model [7] is employed to simulate the combustion processes with high fidelity. This model offers a comprehensive representation of chemical kinetics, enabling accurate predictions of key emission species such as NO_x, unburned hydrocarbons (HC), and carbon monoxide (CO). To improve computational efficiency, the adaptive zoning method [11] is used. This approach groups computational cells with similar temperature and equivalence ratio values into shared zones, allowing them to reuse combustion chemistry calculations, thereby significantly reducing the computational cost while preserving chemical accuracy.

D. Chemical kinetics mechanism selection

The choice of chemical mechanism plays a critical role in accurately predicting ignition behavior and flame propagation. In this study, the GRI-Mech 3.0 [12] mechanism is used for the SAGE simulations. This mechanism includes 53 chemical species and 325 elementary reactions, specifically optimized for modeling methane and small hydrocarbon combustion with detailed NO_x chemistry. To reduce computational cost while maintaining fidelity, heavier hydrocarbon components in the fuel (C4H10, C5H12, C6H14, C7H16) are lumped into propane (C3H8) based on their mass fractions. This simplification is justified by the relatively small concentrations of these heavier species in the fuel and helps accelerate convergence in the combustion simulation without significantly compromising accuracy.

E. Numerical method

Transport equations were solved using the Pressure-Implicit with Splitting of Operators (PISO) method [13]. A first-order upwind spatial discretization scheme was applied to the momentum, energy, density, species, and turbulence transport equations. Time integration was performed using a first-order backward Euler implicit scheme. The Redlich–Kwong equation of state was used for the gas phase, and thermal properties such as species diffusivity, viscosity, and thermal conductivity were calculated based on single-species transport properties (assumes the temperature-dependent transport properties are the same for all species). To capture the detailed dynamics of flame development—and recognizing that real gas flaring is inherently unsteady—the simulations were performed using a fully transient solver.

F. Methane Destruction & Removal Efficiency calculation

The Destruction and Removal Efficiency (DRE) is a key performance metric for evaluating gas flares. It quantifies the flare's ability to eliminate methane emissions by accounting for the fraction of the fuel that is thermally destroyed and prevented from being released into the atmosphere. A high DRE indicates effective combustion and minimal environmental impact. In this study, the DRE is defined as:

$$DRE = 1 - \frac{\dot{m}_{CH_4,outlet}}{\dot{m}_{CH_4,inflow}} \tag{1}$$

where $\dot{m}_{CH_4,outlet}$ is the flow rate of the CH4 mass out of the calculation domain, and $\dot{m}_{CH_4,inflow}$ is the CH4 mass flow rate entering from the HP inflow boundary.

IV. RESULTS AND DISCUSSION

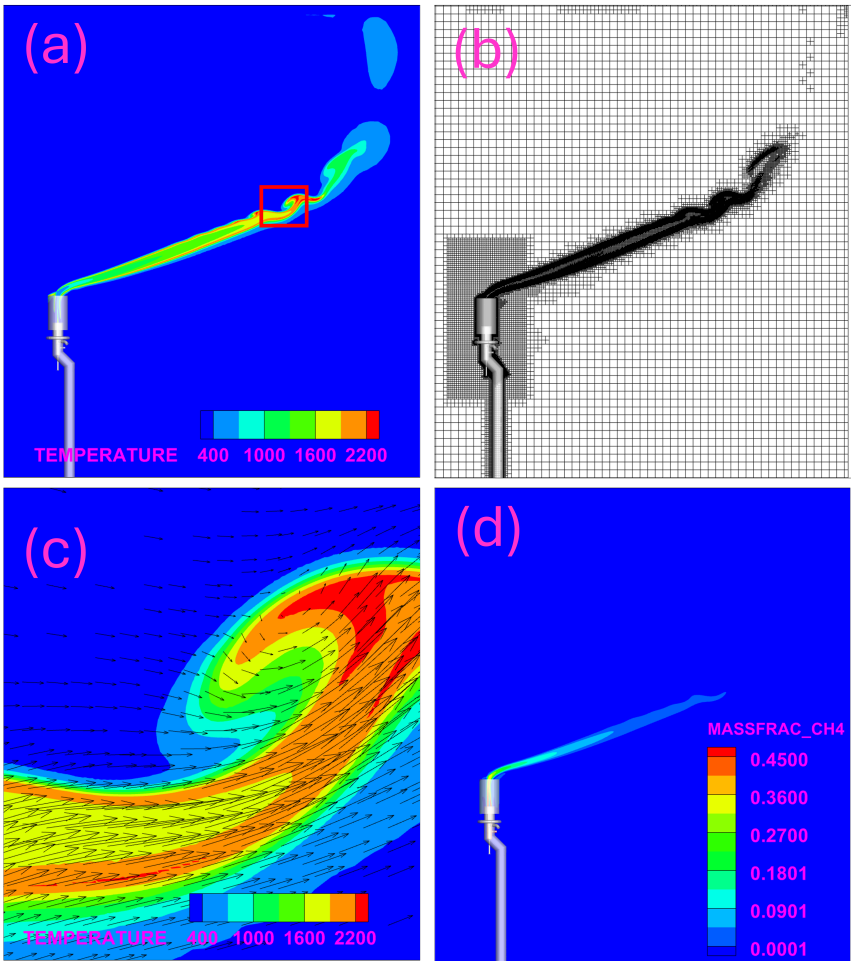

FIG. 3: Simulation results reach quasi-steady state with 30% stoichiometric air and a 10 mph wind flowing from left to right: (a) temperature field; (b) mesh at current step; (c) tangential velocity field zoomed in on the flame region shown in (a); (d) CH4 mass fraction.

This section presents the simulation results and discusses the influence of air supply and environmental conditions on flare performance, with a particular focus on the DRE of methane. First, we describe the general flame characteristics observed under baseline conditions, including the effects of wind and passive air inflow on flame structure. Next, we examine how DRE varies as a function of sampling distance, which is important for both experimental validation and consistent numerical evaluation. Finally, we analyze the impact of air supply rate on flame stability and DRE, highlighting the negative effects of over-aeration, including reduced combustion efficiency and potential flame blowout at high air-to-fuel ratios.

The results in Fig. 3 illustrate the key flow and combustion features of the baseline case with 30% air supply and a 10 mph crosswind. This air supply level was selected as the baseline because, across most conditions, it consistently demonstrated high methane DRE. Fig. 3(a) shows the temperature field, where the flame adopts a conical shape that is tilted to the right, reflecting the influence of the wind. The flame remains attached to the flare tip with a stable, high-temperature core, indicating consistent combustion despite the low air supply. Fig. 3(b) displays the computational mesh in the symmetry plane, which combines AMR and local fixed embedding. The AMR capability dynamically refines the mesh in regions with strong gradients—such as the flame front, shear layers, and jet–air interface—ensuring accurate resolution of combustion and mixing phenomena. In addition, fixed embedding is used

to statically refine critical areas near the flare tip and base of the flame to guarantee sufficient resolution throughout the simulation. Fig. 3(c) presents the velocity field, where the interaction between the fuel jet and crosswind generates strong velocity gradients and promotes shear-layer mixing. This mixing enhances passive air entrainment, facilitating fuel–air interaction and oxidation. Fig. 3(d) shows the methane mass fraction, where CH4 is rapidly consumed along the flame path. Only negligible amounts of methane reach the outlet, supporting the calculated DRE of 99.96%. Together, these figures confirm that effective combustion and high methane abatement are achieved through a combination of passive air entrainment and wind-induced mixing.

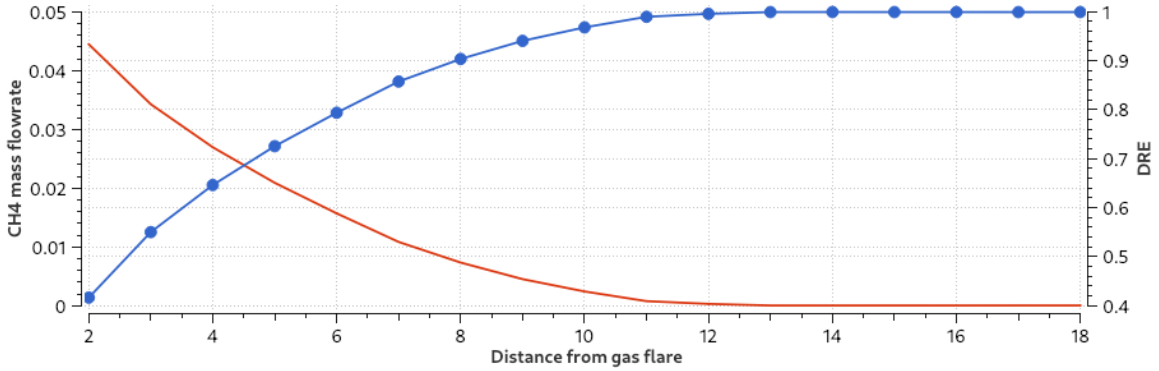

FIG. 4: Variation of DRE as a function of downwind distance from the flare with 30% stoichiometric air and a 10 mph wind speed. The red curve shows the flow rate of CH4 at different location, while the blue curve, marked with circles, represents the calculated DRE of CH4.

The location at which the DRE is evaluated plays a critical role in ensuring accurate and meaningful results. In both experimental measurements (e.g., passive FTIR [6]) and numerical simulations, it is essential to select a position that is sufficiently far downstream from the flare tip to ensure that combustion has completed and the residual methane concentration has stabilized. If DRE is evaluated too close to the flame, the result may underestimate the actual performance due to the presence of unburned CH4 still undergoing oxidation. Fig. 4 presents the DRE as a function of downwind distance from the flare with 30% stoichiometric air and a 10 mph wind speed, based on data extracted along the centerline of the computational domain. The results show that the DRE increases rapidly within the near field of the flame and gradually plateaus beyond a certain distance, indicating the completion of CH4 oxidation. Based on this trend, 14 meters downstream from the flare was selected as the reference location for DRE evaluation for this particular test case. At this point, the methane concentration has leveled off with no significant changes observed further downstream. This also validates that the computational domain size is sufficiently large, ensuring that the simulation captures the full extent of the combustion process and that the outlet boundary does not artificially influence the calculated DRE.

Fig. 5 illustrates the impact of over-aeration on flame stability and methane destruction efficiency under four different stoichiometric air supply conditions: 30%, 50%, 100%, and 150%. It is noted that additional air is entrained into the flame from the ambient environment beyond the forced assist air. At 30% air supply, the flame is stable, well-anchored at the flare tip, and fully contained within the cylindrical shroud, yielding the highest CH4 DRE of 99.96%. When the air supply increases to 50%, the velocity within the shroud—particularly near the iso-surface where the reaction ratio approaches unity—exceeds 5 m/s. This velocity surpasses the local flame speed for CH4, causing the flame to be pushed partially outside the shroud, although it remains attached to the flare tip. The DRE under this condition drops slightly to 99.5%. At 100% air supply, even the velocity near the flare tip exceeds the flame speed, leading to flame lift-off and detachment from the flare. Combustion is still sustained due to the fixed fuel flow and crosswind, but the DRE drops significantly to 47.5%. At 150% air supply, the over-aeration becomes excessive, and the flame is completely blown out due to the high strain induced by the elevated air velocity, indicating a failure to sustain combustion at such high air-to-fuel ratios. The last column in Fig. 5 shows the CH4 mass fraction for each case, clearly indicating reduced combustion efficiency with increasing air supply.

V. CONCLUSION

This study utilized CFD simulations to examine the combustion performance and methane destruction efficiency of the Cimarron hybrid tandem gas flare under varying stoichiometric air supply rates. The results demonstrated that optimal assist air supply is crucial for maintaining stable flame attachment and achieving high Destruction and Removal Efficiency (DRE). At 30% and 50% stoichiometric air—both within the generally accepted optimal

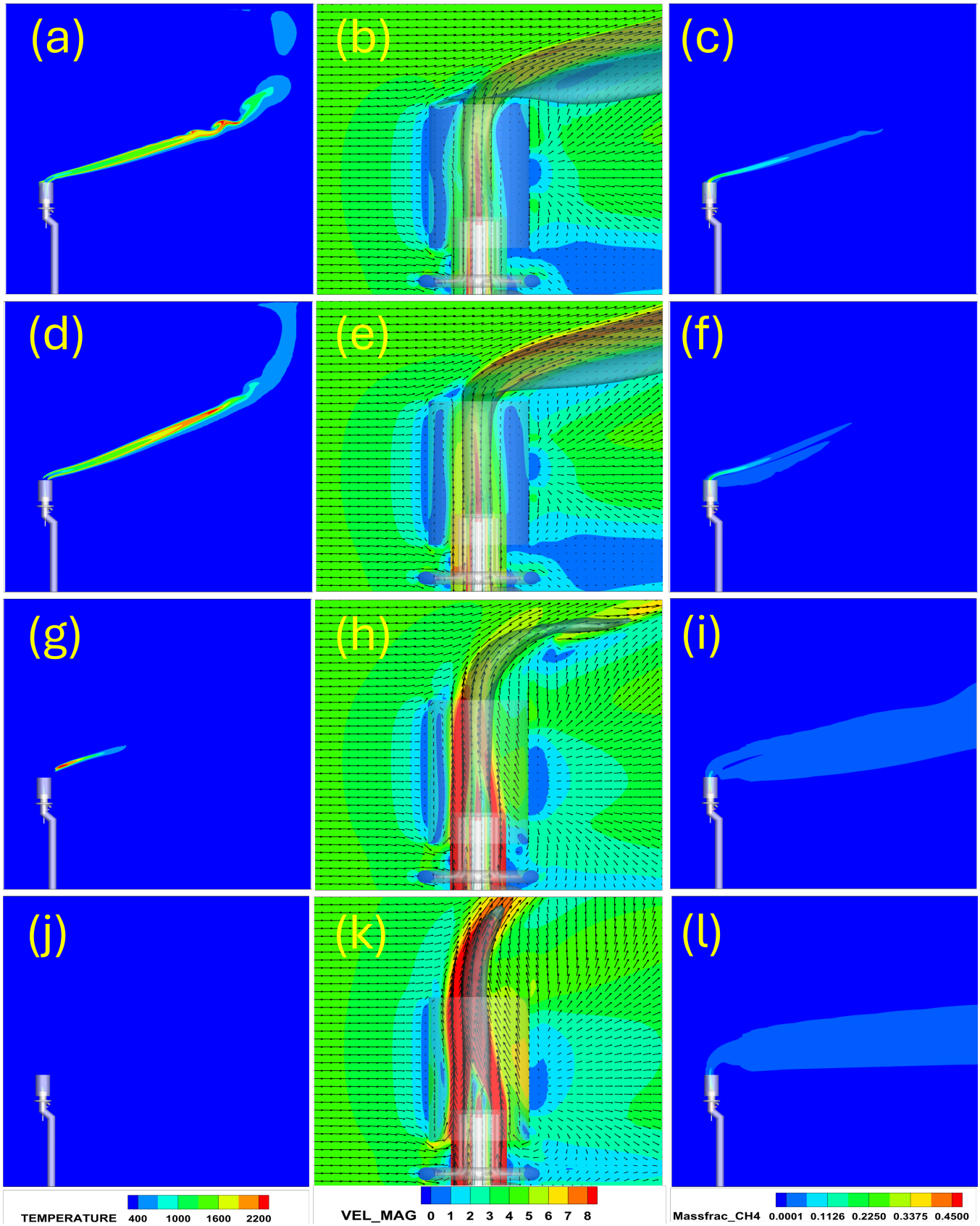

FIG. 5: Transient simulation results which reach quasi-steady under varying stoichiometric air supply: 30% (top row), 50% (second row), 100% (third row), and 150% (bottom row). For each condition, the temperature field (left column), tangential velocity field (middle column), and CH4 mass fraction field (right column) are shown. An iso-surface corresponding to a reaction ratio of 1—indicating regions of well-mixed fuel and air—is overlaid on the velocity fields. Panels: (a–c) 30% air supply; (d–f) 50% air supply; (g–i) 100% air supply; (j–l) 150% air supply. Note: Air supply here is the active air delivered through the assist tube, additional air is also introduced through passive inlets around the shroud, and through entrainment from the surrounding environment.

range for air-assisted gas flares—the flare exhibited a stable flame and achieved methane DRE of 99.96% and 99.5%, respectively, consistent with experimental results from Cimarron's REMEDY program reporting DRE above 99.5%. The analysis also highlighted that the downstream location for DRE evaluation should be carefully selected to ensure complete oxidation of methane within the simulation domain. For this particular test condition, a distance of 14 meters from the flare tip was sufficient, beyond which the calculated DRE remained unchanged. Increasing the assist air supply beyond optimal levels led to over-aeration, causing elevated flow velocities that exceeded the flame speed. This resulted in flame lift-off, significant reductions in methane destruction efficiency, and eventual flame blowout at very high air-to-fuel flow rates. These findings emphasize the need for careful control of assisted air delivery to optimize flare stability and methane destruction efficiency, providing valuable guidance for improving air-assisted flare operation, reducing methane emissions, and supporting compliance with environmental regulations. This also highlights the potential of using high-fidelity CFD to accurately predict DRE, which can aid in reducing the costs associated with design modifications and testing.

[1] Emam, E. A. (2015). GAS FLARING IN INDUSTRY: AN OVERVIEW. Petroleum & coal, 57(5).

[2] Castineira, D., Edgar, T. F. (2006). CFD for simulation of steam-assisted and air-assisted flare combustion systems. Energy & fuels, 20(3), 1044-1056.

[3] Maaroof, A. A., Smith, J. D., Zangana, M. H. (2024). A New Air-Assisted Flare Tip Design for Managing Gas Flare Emissions (CFD Analysis). Processes, 12(9), 1834.

[4] Hong, J. (2021) Minimizing Fugitive Emissions from Air Flares Used in Upstream Applications, Fugitive Emissions Journal.

[5] Hong J. (2021) US patent 11,067,272 Tandem Flare, US Patent and Trademark Office.

[6] Hong, J. (2023). Enhanced Destruction and Removal Efficiency in Air Assisted Flares: Cimarron's DreamDuo and DRE-Max VFD Controller Integration, AFRC.

[7] Richards, K.J., Senecal, P.K. and Pomraning, E. CONVERGE 4. (2024).

[8] Yakhot, V., Orszag, S. A. (1986). Renormalization group analysis of turbulence. I. Basic theory. Journal of scientific computing, 1(1), 3-51.

[9] Amsden, A.A. (1997) " KIVA-3V: A Block Structured KIVA Program for Engines with Vertical or Canted Valves," Los Alamos National Laboratory Technical Report LA-13313-MS.

[10] Launder, B. E., Spalding, D. B. (1983). The numerical computation of turbulent flows. In Numerical prediction of flow, heat transfer, turbulence and combustion (pp. 96-116). Pergamon.

[11] Raju, M., Wang, M., Dai, M., Piggott, W. et al., (2012) Acceleration of Detailed Chemical Kinetics Using Multi-zone Modeling for CFD in Internal Combustion Engine Simulations, SAE Technical Paper 2012-01- 0135.

[12] Gregory P. Smith, David M. Golden, Michael Frenklach, Nigel W. Moriarty, Boris Eiteneer, Mikhail Goldenberg, C. Thomas Bowman, Ronald K. Hanson, Soonho Song, William C. Gardiner, Jr., Vitali V. Lissianski, and Zhiwei Qin $http://www.me.berkeley.edu/gri\_mech/$

[13] Issa, R. I. (1986). Solution of the implicitly discretised fluid flow equations by operator-splitting. Journal of computational physics, 62(1), 40-65.